Title	Relation of crack-induced current shunting to transport current and n-value in DyBCO-coated superconductor
Author(s)	Ochiai, S.; Okuda, H.; Arai, T.; Nagano, S.; Sugano, M.; Osamura, K.; Prusseit, W.
Citation	Cryogenics (2011), 51(10): 584-590
Issue Date	2011-10
URL	http://hdl.handle.net/2433/150119
Right	© 2011 Elsevier Ltd.
Type	Journal Article
Textversion	author

Relation of crack-induced current shunting to transport current and *n*-value in DyBCO-coated superconductor

S. Ochiai[a,*], H. Okuda[a], T. Arai[a], S. Nagano[a], M. Sugano[b], K. Osamura[c] and W. Prusseit[d]

[a] *Department of Materials Science and Engineering, Kyoto University, Sakyo-ku, Kyoto 606-8501, Japan*

[b] *High Energy Accelerator Research Organization (KEK), Cryogenics Science Center, J-PARC Center, 203-1 Shirakata, Tokai-Mura, Naka-gun, Ibaraki 319-1106, Japan*

[c] *Research Institute for Applied Sciences, Sakyo-ku, Kyoto 606-8202, Japan*

[d] *THEVA Dünnschichttechnik GmbH, Rote-Kreuz-Straße 8, 85737 Ismaning, Germany*

Abstract

Transport current and *n*-value of DyBCO–coated conductor pulled in tension were measured experimentally and their relation to crack-induced current shunting was analyzed with the partial crack-current shunting model. The following features were revealed. The shunting current increases with increasing transport current and with increasing crack size. At low voltage where shunting current is low, the transport current of cracked sample normalized with respect to the transport current in non-cracked state is described with the modified ratio of non-cracked area to overall cross-sectional area of superconducting layer. At high voltage where the shunting current is high, the normalized transport current becomes higher than the modified ratio of non-cracked area. The increase in shunting current with transport current (and voltage) leads to a decrease in *n*-value at high current (voltage). This phenomenon is enhanced by crack extension.

Keywords: Superconductors (A); Critical current density (C); Stress effects (C)

* Corresponding author. Address: Department of Materials Science and Engineering, Graduate School of Engineering, Kyoto University, Yoshida, Sakyo-ku, Kyoto 606-8501, Japan. Tel.:+81 75 753 4834; fax: +81 75 753 4841

E-mail address: shojiro.ochiai@materials.mbox.media.kyoto-u.ac.jp (S. Ochiai)

1. Introduction

During fabrication and in service, coated conductor tapes such as RE(Y, Sm, Dy)$Ba_2Cu_3O_{7-\delta}$ systems as well as filamentary composite tapes such as $Bi_2Sr_2Ca_2Cu_3O_{10+x}$ (Bi2223), Nb_3Sn and MgB_2 systems are subjected to thermal, mechanical and electromagnetic stresses. When the subjected stress/strain is high, the superconducting layer/filament is cracked, resulting in loss of the superconducting properties in both coated [1-7] and filamentary [8-16] tapes. For safe and reliability design, it is required to describe the relation of cracks in coated layer to superconducting properties.

The thermal, mechanical and electromagnetic stresses are three-dimensional in nature, but since the failure mechanism is transverse crack formation in most cases, the experimental work is done using uni-axial strain only. The voltage (V) - current (I) relation under an existent partial crack in a BSCCO filament embedded in stabilizer has been modeled by Fang et al [8]. Here, "partial crack" means the crack that exists in a part of transverse cross-section of the superconducting phase. Shin et al [14] have found that the measured V-I curves and change in critical current I_c as a function of applied tensile strain ε_T in BSCCO composite tape can be described with this model by using an effective relative crack size (ratio of the cracked cross-sectional area to overall transverse cross-sectional area) as a fitting parameter. Miyoshi et al [16] have applied this model to the V-I curves of the Nb_3Sn filamentary composite tape containing collective cracks (cracks composed of successively fractured filaments in a transverse cross-section), and have found that this model captures the effect of diminishing I_c as a function of fractional decrease in the number of intact filaments. Recently, the authors [6] applied this model to analysis of V-I curve and to estimation of critical current I_c and n-value in the $DyBa_2Cu_3O_{7-\delta}$ (DyBCO) coated conductor, since the current-shunting mechanism under existent cracks is common in both filamentary and coated conductors despite the difference in geometry. The measured V-I curves, critical currents and n-values at various applied strains were described well by this model.

In the present work, the model of Fang et al [8] was extensively used to analyze the relation of transport current and n-value to shunting current in the voltage range of V=0.15~15 μV (corresponding to 0.1-10 μV/cm) in DyBCO-coated conductor. The analyzed results in

comparison with the experimental ones are presented in this paper.

2. Procedures for experiment and analysis

The DyBCO coated conductor, whose fabrication procedure has been shown elsewhere [17], was supplied by THEVA, Germany. The as-supplied sample consisted of Hastelloy C-276 substrate (thickness 90 μm), MgO buffer layer (3.3 μm) deposited by inclined substrate deposition (ISD) process, MgO cap layer (0.3 μm), DyBCO superconducting layer (2.5 μm) and Ag contact layer (0.5 μm). The as-supplied sample was electro-plated with copper at Kyoto University at room temperature with an electrolyte composed of $CuSO_4$:210g/l, H_2SO_4: 52.4g/l and pure water. The thickness of the plated copper layer was 60 μm. The copper-plated sample was used for experiment, and the results were analyzed.

The voltage taps for measurement of the *V-I* curves were soldered with a spacing of L=15 mm. The *V-I* curves under various applied strains were measured with the usual four-probe method at 77K in a self magnetic field. The *V-I* curve was approximated by

$$V = AI^n \qquad (1)$$

where n and A are the fitting constants. The n-value was estimated for the voltage range of V =0.15-15 μV(0.1-10μV/cm). Thus estimated n-value is, hereafter, noted as n(0.15-15 μV). The critical current I_c was estimated at a voltage of $V=V_c=LE_c$=1.5 μV where E_c(=1 μV/cm in this work) is the electrical field criterion for critical current.

The partial crack-current shunting model of Fang et al [8] was used for analysis of *V-I* curve of cracked DyBCO coated conductor, as in the preceding work [6]. Figure 1 shows a schematic representation of (a) current path and (b) simplified electrical circuit under an existent partial crack in DyBCO layer. In the present DyBCO coated conductor sample, DyBCO layer exhibits arrayed multiple cracks due to the Lüder's deformation of Hastelloy C-276 alloy [3,6], as shown in Fig.2. The cracks are small in size in the early stage. They extend in transverse direction with increasing applied strain. In the preceding work [6], we replaced the arrayed multiple cracks by a single equivalent crack in application of the model, since the shunting of current occurs in the same mechanism in both single and multiple cracks.

The experimental results were described well by this replacement. Based on this result, multiple cracks were replaced by a single equivalent crack also in this work, as shown in Fig.1(a).

In the transverse cross-section in which a partial crack exists, the cracked part in Fig.1(a) losing superconductivity and ligament (non-cracked) part keeping superconductivity co-exist. We define the ratio of cross-sectional area of cracked part to overall cross-sectional area of DyBCO layer as f. The ligament part with an area ratio 1-f transports current I_d through DyBCO layer. At the cracked part with an area ratio f, current I_s (=I-I_d) shunts into Ag and Cu layers. In the shunting circuit, the electrical resistances at the DyBCO-Ag and Ag-Cu interfaces and resistances in Ag and Cu are included in the total resistance R_t (Fig.1(b)). The voltage developed in the ligament part that transports current I_d is noted as V_d. The voltage V_s=$I_s R_t$, developed in the cracked part by shunting current I_s, is equal to V_d since the ligament- and cracked parts constitute of a parallel circuit.

The V-I relation of non-cracked DyBCO layer with a critical current I_{c0} is expressed as

$$V = E_c L\left(\frac{I}{I_{c0}}\right)^{n_0} \qquad (2)$$

where L is the distance between the voltage taps (15 mm in this work), E_c is the electric field criterion for critical current (1μV/cm), and n_0 is the n(0.15-15μV)-value in non-cracked state.

The voltage V_d developed in the ligament part is given by V_d=$E_c s[I_d/\{(I_{c0}(1\text{-}f))\}]^{n_0}$ [8], where s is the crack width. The overall voltage V is given by the sum of the voltage along the length of L-s in the non-cracked region and the voltage along the length s in the cracked region. Due to $s << L$, the overall voltage V is expressed as

$$V = E_c L\left(\frac{I}{I_{c0}}\right)^{n_0} + V_d \qquad (3)$$

The voltage V_d is equal to V_s (=$I_s R_t$), as stated above. The transport current I is the sum of the DyBCO ligament-transported current I_d and shunting current I_s, and is expressed as [8]

$$I = I_{\mathrm{d}} + I_{\mathrm{s}} = I_{\mathrm{c0}}\left(1-f\right)\left[\frac{V_{\mathrm{d}}}{E_{\mathrm{c}}s}\right]^{\frac{1}{n_0}} + \frac{V_{\mathrm{d}}}{R_{\mathrm{t}}} \qquad (4)$$

Equation (4) is modified into the following form [6],

$$I = I_{\mathrm{d}} + I_{\mathrm{s}} = I_{\mathrm{c0}}\left(1-f\right)\left(\frac{L}{s}\right)^{\frac{1}{n_0}}\left[\frac{V_{\mathrm{d}}}{E_{\mathrm{c}}L}\right]^{\frac{1}{n_0}} + \frac{V_{\mathrm{d}}}{R_{\mathrm{t}}} \qquad (5)$$

As has been shown in our preceding work [6], the term $(1\text{-}f)\ (L/s)^{1/n_0}$ in Eq.(5) is the modified ratio of non-cracked area. This term and R_t can be obtained by fitting Eqs.(3) and (5) to the measured *V-I* curves. Once they are obtained, we can estimate I_d, I_s and $V_d(=V_s)$ as a function of transport current I (and voltage V) [6].

3. Results and Discussion

3.1 Experimental results

Figure 3 shows the measured *V-I* curves in logarithmic scale at various applied tensile strains (ε_Γ). From the *V-I* curves, the critical current I_c at $V=V_c=E_cL=1.5$ μV and n(0.15-15 μV)-value in the voltage range of $V=0.15$ to 15 μV were measured, as shown in Fig.4(a) and (b), respectively. The correlation of n(0.15-15 μV) to critical current I_c is shown in Fig.4(c). It is clearly shown that both I_c and n(0.15-15 μV) decrease significantly at high ε_Γ (Fig.4(a) and (b)) and the lower the I_c, the lower becomes the n(0.15-15 μV) (Fig.4(c)).

The sharp decreases in I_c and n(0.15-15 μV) beyond $\varepsilon_\Gamma=0.37\%$ stem from cracking in the DyBCO layer [6]. The ranges of ε_Γ in non-cracked and cracked states in the present copper-plated sample are shown in Fig.4. For analysis of *V-I* curves with Eqs.(3) and (5) of cracked samples strained more than 0.37%, we need the original critical current I_{c0} under a

criterion of E_c=1 μV/cm and original n-value, n_0, estimated in the voltage range of 0.15 to 15 μV in non-cracked state. The I_{c0} and n_0 for analysis were obtained as follows. The monotonic decrease in I_{c0} with ε_T in the non-cracked range (0.1%<ε_T<0.37%) in Fig.4(a) was empirically expressed as

$$I_{c0}=199.4-14.3\varepsilon_T \quad (\varepsilon_T:\%) \qquad (6)$$

As an approximation, the I_{c0} value, obtained by the extrapolation of Eq.(6) to each tested strain ε_T(>0.37%), was used as I_{c0} in the present analysis. The strain dependence of n(0.15-15 μV)-value in the non-cracked strain range (ε_T<0.37%) was not large in comparison with that in cracked range (ε_T>0.37%) as in Fig.4(b). The n_0-value was taken from the average of the n(0.15-15 μV)-values in the strain range of 0.1%<ε_T<0.37% in Fig.4(b); n_0=42.1.

3.2 Estimation of $(1-f)(L/s)^{1/n_0}$ and R_t

The values of $(1-f)(L/s)^{1/n_0}$ and R_t, obtained by fitting the measured V-I curves (Fig.3) to Eqs.(3) and (5) with n_0=42.1 and I_{c0} (obtained by substituting the corresponding ε_T into Eq.(6)), are shown in Fig.5. To examine the reproducibility of V-I curves with the estimated values of $(1-f)(L/s)^{1/n_0}$ and R_t, the V-I curve at each ε_T was back-calculated by substituting the estimated values into Eqs.(3) and (5). As shown in Fig.6, the V-I curves were reproduced successfully. Also using the reproduced V-I curves, we obtained the critical current I_c and n(0.15-15 μV)-values, as shown with open triangles in Fig.4. The experimental results (open circles) were reproduced well. Based on these results, the estimated values of $(1-f)(L/s)^{1/n_0}$ and R_t were used to derive I_s and V_d, as follows.

3.3 Estimation of shunting current I_s

Fig.7 (a) shows an example of the calculated change in shunting current I_s (solid curve) and DyBCO ligament-transported current I_d (dotted curve) as a function of total transport current I, together with the calculated values of I, I_s and I_d at V=1.5, 7.5 and 15 μV. In this example, the data of the sample strained by ε_T=0.449%, whose measured and calculated V-I curves are shown in Fig.6 and the values of $(1-f)(L/s)^{1/n_0}$ and R_t are shown in Fig.5, is taken up representatively. At low I (and low V), shunting current I_s is low, while the DyBCO ligament-transported current I_d is on high level. The total current is almost determined by I_d in low I (low V) range. On the other hand, I_s increases largely beyond around I_c (102.1 A) at V=1.5 μV in contrast to the gradual increase in I_d; I_s increases from 1.9 A at V=1.5 μV to 18.8 A at V=15 μV, while I_d increases only by 4.7 A in the range of V=1.5 to 15 μV. Accordingly, the ratio of I_s to I, I_s/I, increases with I especially beyond I=I_c (i.e. beyond V=V_c(=LE_c=1.5 μV)).

In the same way, the I_s/I values at V=1.5, 7.5 and 15 μV at each ε_T tested were calculated and plotted against ε_T, as shown in Fig.7(b). The variations of measured I values at 1.5, 7.5 and 15 μV with ε_T are also shown for reference. The following features are read. (1) The I_s/I increases and I decreases with increasing ε_T at any V, indicating that I_s/I becomes larger when the sample is more severely cracked. (2) I_s/I increases with increasing V in all samples. I_s/I at V=15 μV is around 10 times higher than that at V=1.5 μV.

3.4 Estimation of voltage V_d(=V_s) developed at cracked region

Figure 8(a) shows two examples of V-I and V_d-I curves in normal scale, calculated by substituting the $(1-f)(L/s)^{1/n_0}$ and R_t values shown in Fig.5 into Eqs.(3) and (5). Example 1 shows the case strained by ε_T=0.382%, whose I_c and I_{c0} are 180.4 A(calculated by Eqs.(3) and (5)) and 193.9 A (calculated by Eq.(6)), respectively. The critical current I_c is by 7% reduced from I_{c0} by cracking. V_d values are read to be 1.43, 6.89 and 12.7 μV at V=1.5, 7.5 and 15 μV, respectively. The ratios of V_d to V, V_d/V, are 0.95, 0.92 and 0.85, respectively. The result of

this example means that (1) the contribution of the term $E_cL(I/I_{c0})^{n_0}$ to total V is small (Eq.(3)) and most voltage is generated at the cracked region even though the damage is small ($(1-f)(L/s)^{1/n_0}$=0.93) and (2) V_d/V decreases with increasing V (and I) due to the enhanced current shunting at high V. On the other hand, in the example 2 strained by ε_T=0.394% where I_c (161.6 A) is by 17% reduced from I_{c0}(193.8 A), V_d at any V is almost equal to V (the V-I and V_d-I curves are almost overlapped in this example). This means that the overall voltage stems from the voltage developed at the cracked region when crack extends more ($(1-f)(L/s)^{1/n_0}$ is reduced from 0.93 at ε_T=0.382% to 0.83 at ε_T=0.394%).

In the same way, the V_d/V at V=1.5, 7.5 and 15 μV at each ε_T was calculated and plotted against ε_T, as shown in Fig.8(b). Except the V_d/V values at ε_T=0.382%, the V_d/V values were unity regardless the values of V and ε_T. Only the case at ε_T=0.382%, which had the highest I_c value in the cracked range in the present work, had the V_d/V values (0.95, 0.92 and 0.85 at V=1.5, 7.5 and 15 μV, respectively) slightly smaller than unity. This result shows that the total voltage V in the cracked sample stems mostly from the cracked region and the contribution of $E_cL(I/I_{c0})^{n_0}$ in Eq.(3) is small. Consequently, V_d=V holds over almost the entire strain range where cracking occurs.

3.5 Analysis of current I at V=1.5, 7.5 and 15 μV

As has been shown in Fig.4(a), the measured critical current (I_c) values at V=1.5 μV(=1 μV/cm) where I_s/I (=I_s/I_c) is less than several percent (Fig.7(b)) are reproduced well by the estimated values of $(1-f)(L/s)^{1/n_0}$ and R_t. In this subsection, first, whether the total current I(=I_d+I_s) at V=7.5 and 15 μV, where I_s/I is high, can be described by Eqs.(3) and (5) with the estimated values of $(1-f)(L/s)^{1/n_0}$ and R_t or not was examined. Substituting the values of $(1-f)(L/s)^{1/n_0}$ and R_t shown in Fig.5, n_0=42.1, and I_{c0} obtained by Eq.(6) with the corresponding ε_T value into Eqs.(3) and (5), I values at V=7.5 and 15 μV were calculated for

each sample. The calculated I values at V=7.5 (▲) and 15 μV(■), together with those at V=1.5 μV (●) taken from Fig.4(a) for reference, are shown in Fig.7(b). The measured I values at V=1.5(○), 7.5(Δ) and 15 μV (□) at all tested ε_Γ are well described by the calculation results. It is noted that the influence of increase in I_s on I at high V is included in the calculated values of I in Fig.7(b).

Next, we attempted to extract the influence of current shunting on I by using the result shown in Fig.8(b) where V_d=V holds in wide range of extent of cracking. Substituting V_d=V into Eq.(5), we have a simple expression of I as a function V, $I(V)$, for cracked sample;

$$I(V) = I_{c0}(1-f)\left(\frac{L}{s}\right)^{\frac{1}{n_0}}\left[\frac{V}{E_c L}\right]^{\frac{1}{n_0}} + \frac{V}{R_t} \qquad (7)$$

We define the current at arbitrary voltage V in non-cracked state as $I_0(V)$. Using Eq.(2), we have the relation of $I_0(V)$ to the critical current I_{c0} in the form;

$$\frac{I_0(V)}{I_{c0}} = \left(\frac{V}{E_c L}\right)^{1/n_0} \qquad (8)$$

Substituting I_{c0} derived from Eq.(8) and $V(=V_d)/R_t$=I_s into Eq.(7), we have

$$\frac{I(V)}{I_0(V)} = (1-f)\left(\frac{L}{s}\right)^{1/n_0} + \frac{I_s(V)}{I_0(V)} \qquad (9)$$

The left term $I(V)/I_0(V)$ in Eq.(9) is the current at a voltage V in cracked state, normalized with respect to the current in non-cracked state at the same V. Equation (9) indicates that the normalized current $I(V)/I_0(V)$ is given nearly by $(1-f)(L/s)^{1/n_0}$ at low V where $I_s(V)/I_0(V)$ is small, and it deviates upward from $(1-f)(L/s)^{1/n_0}$ at high V where $I_s(V)/I_0(V)$ is large.

The measured and calculated results of $I(V)$ at V=1.5, 7.5 and 15 μV have been shown in Fig.7(b). $I_0(V)$ can be calculated by Eq.(8). The measured and calculated normalized currents

$I(V)/I_0(V)$ are plotted against $(1-f)(L/s)^{1/n_0}$ in Fig.9. In the case of V=1.5 μV(=1 μV/cm), $I_0(V)$ is I_{c0} and $I(V)$ is I_c, and I_s/I_{c0} is less than I_s/I_c (<around 0.05). Accordingly, I(1.5 μV)/I_0(1.5 μV) is almost linear against $(1-f)(L/s)^{1/n_0}$ with a slope nearly unity; namely I(1.5 μV)/I_0(1.5 μV) is nearly equal to $(1-f)(L/s)^{1/n_0}$. In this way, the value of $(1-f)(L/s)^{1/n_0}$, obtained by curve fitting, can be used directly as a measure of normalized critical current under a criterion of E_c=1 μV/cm. On the other hand, I(7.5 μV)/I_0(7.5 μV) and I(15 μV)/I_0(15 μV) deviate upward from the linear relation due to the enhanced current shunting.

3.6 Analysis of variation of n-value with current I and voltage V

In the present work, n(V=0.15-15 μV) was estimated as the n-index in Eq.(1) for the V-I relation in the range of V=0.15 to 15 μV (corresponding to 0.1 to 10 μV/cm). The measured and calculated values of n(0.15-15 μV) have been shown in Fig.4(b). The experimental results are well reproduced by calculation. This result demonstrates that when the voltage range for estimation of n-value is fixed as in the present work, n-value in a given voltage range can be reproduced by the present approach.

However, as the shunting current I_s increases with increasing I (and V), the n-value is dependent on the V-I range for which n-value is estimated. In a very narrow V-I range, the n-value is expressed as $n=\partial\ln(V)/\partial\ln(I)$, corresponding to the slope of V-I curve in logarithmic scale in Figs.3 and 6. In the case of non-cracked state (sample tested at ε_I=0.362% in Fig.3), the slope is almost constant within the V-I range investigated. On the other hand, in the case of cracked samples, their V-I relations in logarithmic scale are not straight but curved. The slope tends to be smaller with increasing I (and V) due to current shunting. The influences of current shunting on n-value are discussed below by using the two differently defined n-values. One is the n-value (noted as n(1.5-15 μV)) estimated by Eq.(1) in the voltage range of V=1.5 to 15 μV (=1-10 μV/cm) where current shunting is enhanced. Another is the n-value (noted as $n(I)$) estimated from the slope in the range between I-1 and I+1 where voltage increases from $V(I-1)$ (voltage at I-1) to $V(I+1)$ (voltage at I+1).

Figure 10 shows the comparison of the measured n(1.5-15 μV) values with calculated ones, together with measured n(0.15-15 μV) values for comparison. Figure 11 shows examples of variation of $n(I)$-value with current I. Example 1 is taken from the data of the sample strained by ε_T=0.411%, whose measured I_c and n(0.15-15 μV) were 136.5 A and 20.8, respectively. Example 2 is taken from the data of the sample strained by ε_T=0.488%, whose measured I_c and n(0.15-15μV) were 74.0 A and 11.0, respectively. Open circles show the measured values and open rectangles show the calculation result by Eq.(3) and (5) with the $(1-f)(L/s)^{1/n0}$ and R_t values shown in Fig.5. The following indications are read from Figs.10 and 11.

(1)As has been shown in Fig.7, the ratio of shunting current to total current, I_s/I, increases with increasing I especially beyond critical current I_c. From this result, it is expected that the $n(I)$ decreases with increasing I (and V) due to the enhancement of current shunting. The expected decrease in $n(I)$ is actually found in both measured and calculated results in Fig.11.

(2) In Fig.11, although the shunting current is low in the low I (low V) region below I_c, $n(I)$ decreases evidently. $n(I)$ is very sensitive to shunting current and, accordingly, shunting current cannot be ignored for description of $n(I)$ in contrast to critical current.

(3) As $n(I)$ varies with I (and V) (Fig.11), each of n(0.15-15 μV) and n(1.5-15 μV) is obtained as a kind of average of varying $n(I)$ in each corresponding voltage range. Actually the n(0.15-15 μV) values (20.8 and 11.0 for examples 1 and 2, respectively) are around average of the varying $n(I)$-value (Fig.11). The voltage range for determination of n(0.15-15 μV) covers both of high $n(I)$ range below I_c and low $n(I)$ range beyond I_c, while the voltage range for determination of n(1.5-15 μV) covers only low $n(I)$ range beyond I_c. This results in lower n(1.5-15 μV) than n(0.15-15 μV) (Fig.10).

4. Conclusions

(1) The experimental results were analyzed using the model of Fang et al. The experimentally measured variations of V-I curve, critical current and n(0.15-15 μV)-value

with increasing applied strain and the correlation of n(0.15-15 μV)-value to critical current were reproduced well by this model.

(2) The current shunting at cracked part is enhanced with increasing transport current (and voltage) especially beyond the critical current. Due to the increase in shunting current with transport current, $n(I)$-value decreases with increasing current. Such a tendency becomes more dominant with progress of cracking.

(3) At critical current under a criterion of 1 μV/cm, shunting current is low and most of the current is transported by the DyBCO ligament part. As a result, the critical current of cracked sample normalized with respect to that of non-cracked state is described by $(1-f)(L/s)^{1/n_0}$. At higher voltages (5 and 10 μV/cm), the contribution of shunting current to total transport current becomes larger. As a result, the current, normalized with respect to the current of non cracked state, deviates upward from $(1-f)(L/s)^{1/n_0}$.

Acknowledgements

The authors wish to express their gratitude to The Ministry of Education, Culture, Sports, Science, and Technology, Japan, for the grant-in-aid (no. 22360281).

References

[1] Cheggour N, Ekin JW, Thieme CLH, Xie Y-Y, Selvamanickam V, Feenstra R. Reversible axial-strain effect in Y–Ba–Cu–O coated conductors. Supercond Sci Technol 2005;18(12):S319-24.

[2] Shin HS, Kim KH, Dizon JR, Kim TY, Ko RK, Oh SS. The strain effect on critical current in YBCO coated conductors with different stabilizing layers. Supercond Sci Technol 2005;18(12):S364–8.

[3] Sugano M, Osamura K, Prusseit W, Semerad R, Kuroda T, Itoh K, Kiyoshi T. Irreversible strain dependence of critical current in 100 A class coated conductors. IEEE Trans Appl Superond 2005;15(2):3581-4.

[4] Osamura K, Sugano M, Machiya S, Adachi H, Ochiai S, Sato M. Internal residual strain

and critical current maximum off a surrounded Cu stabilized YBCO coated conductor. Supercond Sci Technol 2009;22(6):065001.

[5] van der Laan DC, Ekin JW, Douglas JF, Clickner CC, Stauffer TC, Goodrich LF. Effect of strain, magnetic field and field angle on the critical current density of Y $Ba_2Cu_3O_{7-\delta}$ coated conductors. Supercond Sci Technol 2010;23(7):072001.

[6] Ochiai S, Arai T, Toda A, Okuda H, Sugano M, Osamura K, Prusseit W. Influences of cracking of coated superconducting layer on *V–I* Curve, critical current and *n*-value in DyBCO-coated conductor pulled in tension. J Appl Phys 2010;108(6):063905.

[7] Shin HS, Dedicatoria MJ. Mechanical and transport properties of IBAD/EDDC–SmBCO coated conductor tapes during fatigue loading. Cryogenics 2011;51(6):237-40.

[8] Fang Y, Danyluk S, Lanagan MT. Effects of cracks on critical current density in Ag-sheathed superconductor tape. Cryogenics 1996;36(11):957-62.

[9] Kitaguchi K, Itoh K, Kumakura H, Takeuchi T, Togano K, Wada H. Strain effect in Bi-based oxide/Ag superconducting tapes. IEEE Trans Appl Supercond 2001;11(1):3058-61.

[10] Weijers HW, J. Schwartz J, ten Haken B. Bi-based HTS insert coils at high stress levels. Physica C 2002;372-376(3):1364-7.

[11] Ochiai S, Nagai T, Okuda H, Oh SS, Hojo M, Tanaka M, Sugano M, Osamura K. Tensile damage and its Influence on critical current of Bi2223/Ag superconducting composite tape. Supercond Sci Technol 2003;16(9):988-94.

[12] Katagiri K, Kuroda T, Shin H-S, Hiroi K, Itoh K, Wada H. Miniature round robin test on the bending strain characteristics of Ag/Bi(2223) tapes at room and liquid nitrogen temperatures. Physica C 2005;426-431(2):1200-4.

[13] Otto A, Harley EJ, Marson R. Critical current retention in axially strained reinforced first-generation high-temperature superconducting Bi2223 wire. Supercond Sci Technol 2005;18(12):S308-12.

[14] Shin JK, Ochiai S, Okuda H, Sugano M, Oh SS. Change of the *V–I* curve and critical current with applied tensile strain due to cracking of filaments in Bi2223 composite tape. Supercond Sci Technol 2008;21(11):115007.

[15] Ochiai S, Shin JK, Iwamoto S, Okuda H, Oh SS, Ha DW, Sato M. Residual and fracture strains of Bi2223 filaments and their relation to critical current under applied bending and tensile strains in Bi2223/Ag/Ag alloy composite superconductor. J Appl Phys

2008;103(12):123911.

[16] Miyoshi Y, Van Lanen EPA, Dhallé MMJ, Nijhuis A. Distinct voltage–current characteristics of Nb_3Sn strands with dispersed and collective crack distributions. Supercond Sci Technol 2009;22(8);085009.

[17] Prusseit W, Nemetschek R, Hoffmann C, Sigl G, Lümkemann A, Kinder H. ISD process development for coated conductors. Physica C 2005;426-431(2):866-71.

Figure Captions

Fig.1 Schematic representation of (a) current path and (b) simplified electrical circuit under an existent partial crack.

Fig.2 An example of arrayed multiple cracks in DyBCO layer.

Fig.3 Measured *V*-*I* curves at indicated tensile strain ε_T.

Fig.4 Change in (a) critical current I_c and (b) n(0.15-15 μV) with increasing applied tensile strain ε_T, and (c) correlation of n(0.15-15 μV) to critical current I_c. ○ and Δ show the measured values and the calculated values by Eqs.(3) and (5) with the obtained $(1-f)(L/s)^{1/n_0}$ and R_t values, respectively.

Fig.5 Obtained values of $(1-f)(L/s)^{1/n_0}$ and R_t, plotted against applied tensile strain ε_T.

Fig.6 Typical examples of calculated *V*-*I* curves by substituting the obtained values of $(1-f)(L/s)^{1/n_0}$ and R_t into Eqs.(3) and (5) in comparison with the measured ones. The solid and dotted curves show the measured and calculated ones, respectively.

Fig.7 (a) Calculated change in I_s and I_d as a function of transport current I for the sample strained by ε_T=0.449% as an example. (b) Calculated ratios of I_s to I, I_s/I, together with the measured and calculated values of I at V=1.5, 7.5 and 15 μV for all cracked samples investigated.

Fig.8 (a) Example of the *V*-*I* and V_d-*I* curves and (b) estimated values of V_d/V at V=1.5, 7.5 and 15 μV, plotted against tensile strain ε_T.

Fig.9 Measured and calculated values of normalized current $I(V)/I_0(V)$ of cracked samples plotted against $(1-f)(L/s)^{1/n_0}$. (a) V=1.5 μV. (b) 7.5 μV. (c) 15 μV. The solid lines refer to $I(V)/I_0(V)=(1-f)(L/s)^{1/n_0}$.

Fig.10 Measured and calculated n(1.5-15 μV)-values, together with n(0.15-15 μV)-values for comparison, plotted against tensile strain ε_T.

Fig.11 Examples of variations of the measured and calculated $n(I)$-values with transport current I. (a) Example 1 (ε_T=0.411%) (b)Example 2 (ε_T=0.488%)

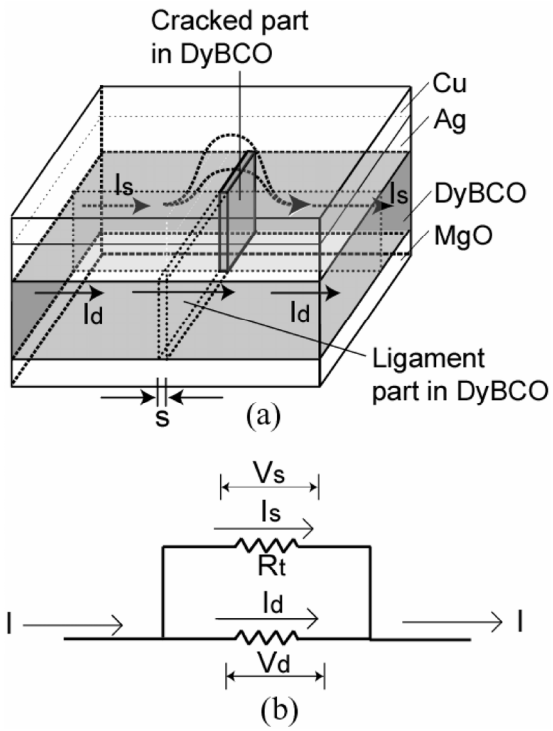

Fig.1

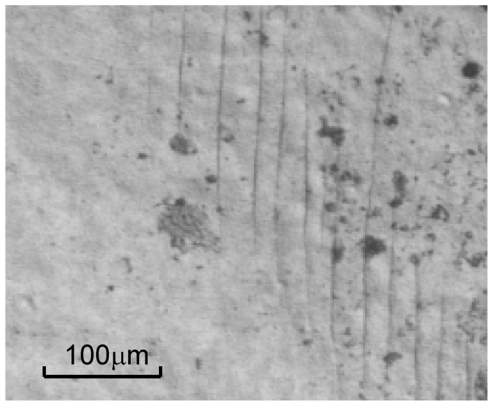

Fig.2

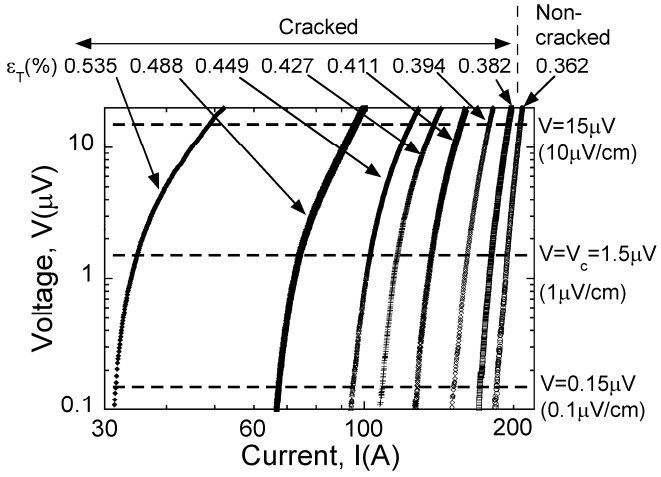

Fig.3

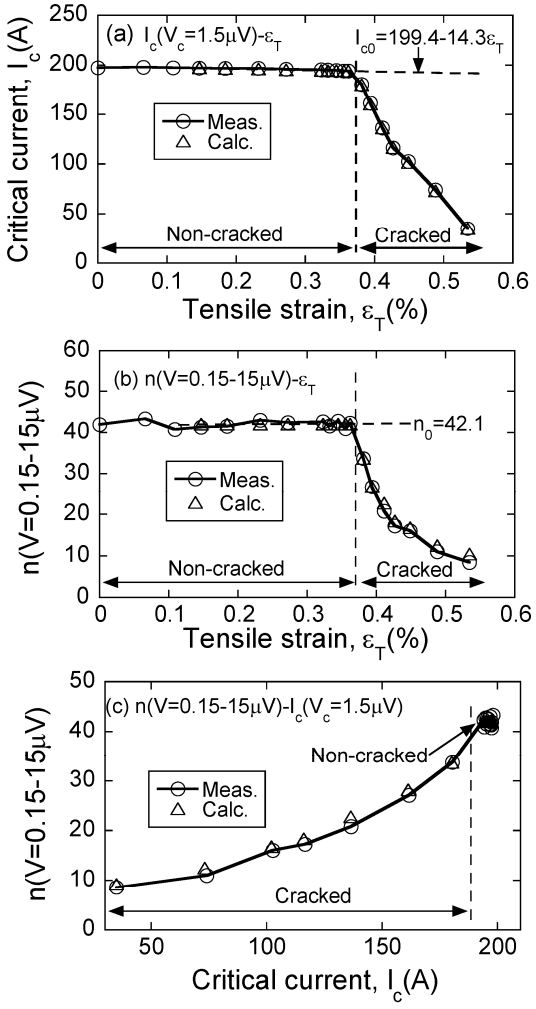

Fig.4

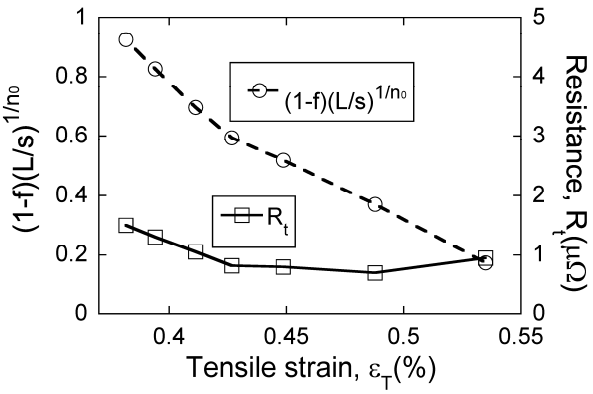

Fig.5

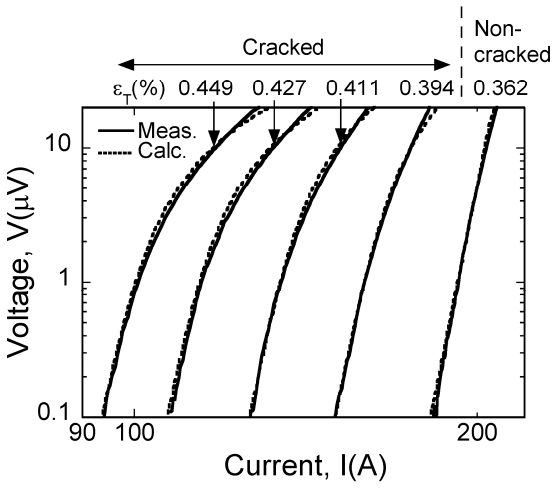

Fig.6

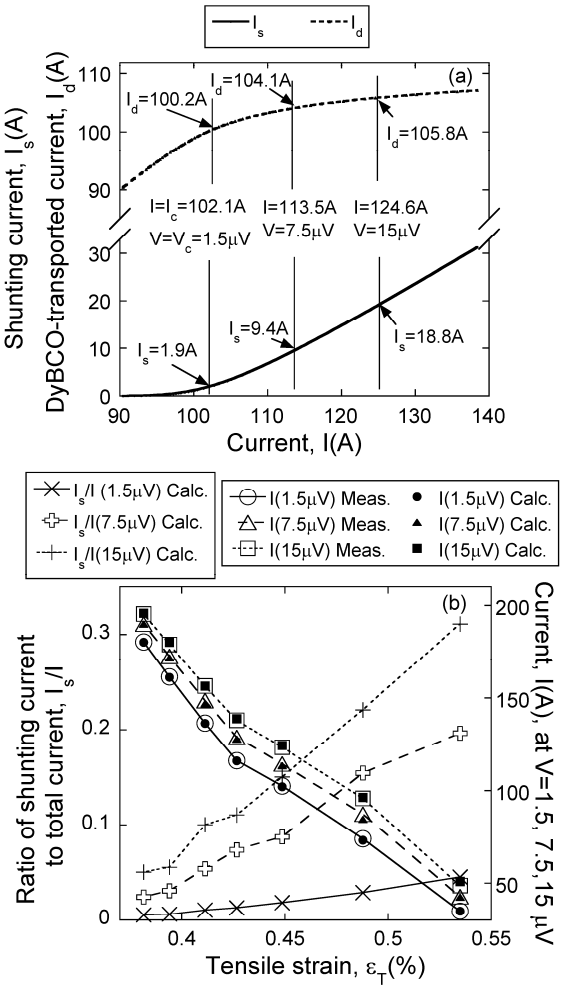

Fig.7

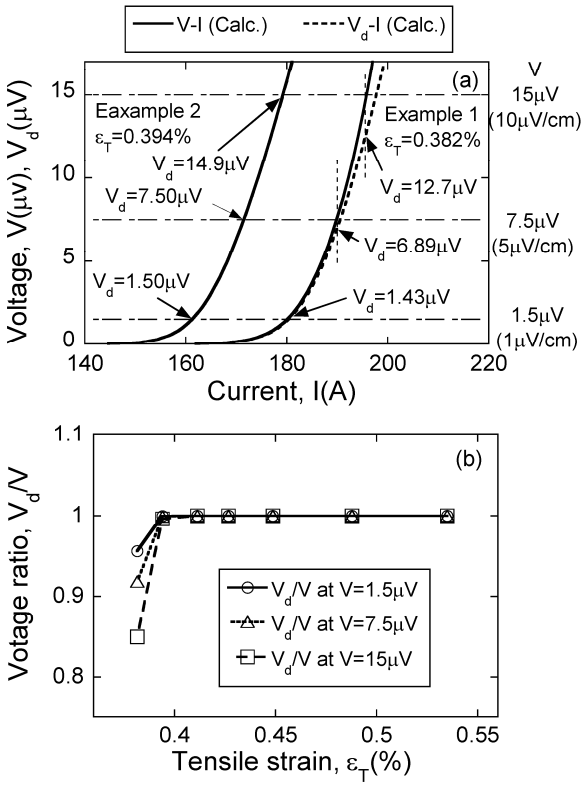

Fig.8

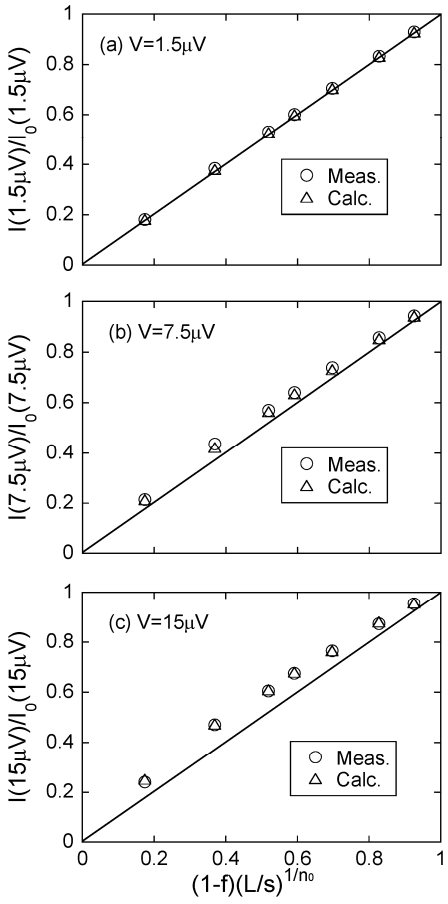

Fig.9

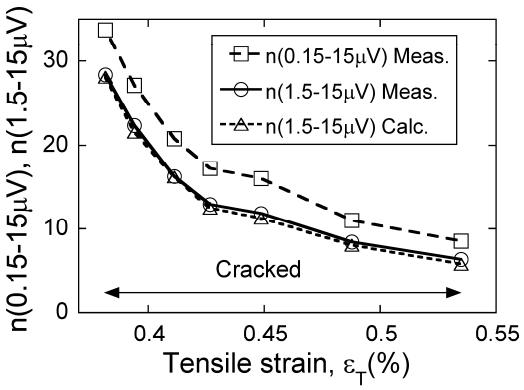

Fig.10

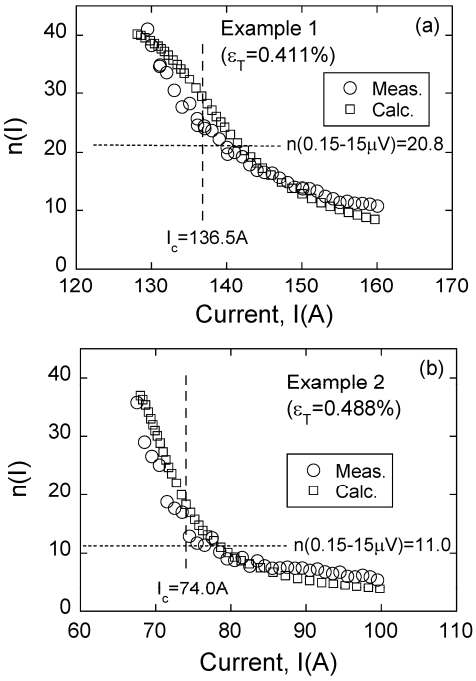

Fig.11